Observed strong atmospheric water constraints on forest photosynthesis using eddy covariance and satellite-based data across the Northern Hemisphere

Yongxian Su, Xueqin Yang, Pierre Gentine, Fabienne Maignan, Jiali Shang, Philippe Ciais

International Journal of Applied Earth Observations and Geoinformation 110 (2022) 102808

Contents lists available at ScienceDirect

International Journal of Applied Earth Observations and Geoinformation

journal homepage: www.elsevier.com/locate/jag

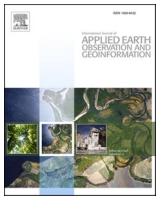

Observed strong atmospheric water constraints on forest photosynthesis using eddy covariance and satellite-based data across the Northern Hemisphere

Yongxian Su [a,b,*], Xueqin Yang [a], Pierre Gentine [c], Fabienne Maignan [b], Jiali Shang [d], Philippe Ciais [b]

[a] Guangdong Provincial Key Laboratory of Remote Sensing and Geographical Information System, Guangdong Open Laboratory of Geospatial Information Technology and Application, Guangzhou Institute of Geography, Guangdong Academy of Science, Guangzhou 510070, China
[b] Laboratoire des Sciences du Climat et de l'Environnement, IPSL, CEA-CNRS-UVSQ, Université Paris-Saclay, 91191 Gif sur Yvette, France
[c] Department of Earth & Environmental Engineering, Columbia University, New York, NY 10027, USA
[d] Ottawa Research and Development Centre, Agriculture and Agri-Food Canada, Ottawa, Ontario, Canada

ARTICLE INFO

Keywords:
Atmospheric water constraint
Soil water constraint
Forest photosynthesis
Northern hemisphere
Climate change

ABSTRACT

Soil water deficit and high atmospheric dryness (vapor pressure deficit, VPD) are major environmental limitations on carbon uptake of terrestrial ecosystems. However, it is still unclear how climate seasonality influences seasonal soil water supply and atmospheric water demand, and consequently limits plant photosynthesis. Here, we analyzed the impacts of the seasonal radiation-rainfall coupling on soil moisture limitations versus atmospheric dryness limitations on plant photosynthesis across the Northern Hemisphere north of 15°N, using the eddy covariance data of 83 forest sites and multiple satellite-based data. Our results show that forest photosynthesis is strongly reduced by low soil water availability that is accompanied by a high atmospheric dryness during warm seasons for sites and regions where there is a strong negative covariation between radiation and rainfall availability, which we denote as asynchronous climate. However, under climates with positive covariation between radiation and rainfall availability, i.e. synchronous climate, forest photosynthesis experiences only a small soil water stress, but tends to be limited by high atmospheric dryness during warm seasons. Both the site and regional analyses imply that atmospheric dryness exhibits stronger constraints on forest photosynthesis in synchronous climate over a larger area than in asynchronous climate across the Northern Hemisphere.

1. Introduction

Soil water deficits and high atmospheric dryness are recognized as two important factors influencing plant phenology and physiology and thus show strong limitation on plant photosynthesis (Zhou et al., 2019b; Novick et al., 2016). These two types of water stresses on photosynthesis are now a key question for understanding terrestrial carbon uptake, energy exchange, and water transfer, which are important for predicting and understanding the impact of climate change on future carbon uptake of terrestrial ecosystems (Cheng et al., 2017; Hartmann, 2009; Liu et al., 2020; Lu et al., 2022; Zhou et al., 2019a).

Soil water is the main reservoir for plant transpiration and surface evaporation (Hartmann, 2009). Soil moisture deficits impede soil and plant hydraulics transport of water from the soil to the leaves (Tyree and Sperry, 1989) and trigger leaf stomata closure to regulate hydraulic conductivity and limit water loss (Martínez-Vilalta et al., 2014; Martínez-Vilalta and Garcia-Forner, 2016) in turn resulting in an inhibition of photosynthesis (Novick et al., 2016). However, even with adequate soil water access for roots, plant stomata tend to close in response to increased atmospheric water demand, i.e., high vapour pressure deficit (VPD) (Novick et al., 2016; Konings et al., 2017). The increased atmospheric water demand forces plant to maximize carbon gains per unit of water loss by inducing some stomatal closure to constrain water loss (Ding et al., 2018; Katul et al., 2009; Sperry et al., 2017). Although soil moisture deficits and high atmospheric dryness both regulate stomatal closure and in turn reduce plant carbon uptake (Konings and Gentine,

* Corresponding author at: Guangdong Provincial Key Laboratory of Remote Sensing and Geographical Information System, Guangdong Open Laboratory of Geospatial Information Technology and Application, Guangzhou Institute of Geography, Guangdong Academy of Science, Guangzhou 510070, China.
E-mail address: suyongxian@gdas.ac.cn (Y. Su).

https://doi.org/10.1016/j.jag.2022.102808
Received 10 March 2022; Received in revised form 30 April 2022; Accepted 30 April 2022
Available online 10 May 2022

2016; Konings et al., 2017), it is still unclear in which climates, soil moisture deficits and high atmospheric dryness act separately or synergistically to inhibit plant photosynthesis.

Here, we hypothesize that, the seasonal phase between incoming radiation (*SW*) and precipitation (*Pre*) controls whether soil water deficit and high atmosphere demand for water happen in the same season or in different seasons, and consequently influences ecosystem-photosynthesis. We investigated this hypothesis using data from 83 eddy-covariance forest sites spanning various ecoregions across Northern Hemisphere (latitude > 15°N) (Fig. 1**A**; Figure S1), as the impacts of environment factors on forests in high latitudes differ greatly from those in mid-to-low latitudes (Messori et al., 2019; Yang et al., 2021). To quantify the seasonal phase between rainfall and radiation availability, we calculated the Pearson correlation coefficients ($R_{climate}$) between monthly means of *SW* and *Pre* during the 1980–2010 period using the method of Yang et al. (2020), who used $R_{climate}$ to evaluate the seasonal phase between rainfall and radiation availability across tropical and subtropical regions. We refer to synchronous climates where *Pre* and *SW* covary positively ($R_{climate} > 0$) and asynchronous climates where *Pre* and *SW* covary negatively ($R_{climate} < 0$) (Yang et al., 2021). To quantify the seasonal co-occurrence between soil water availability and atmospheric dryness, we used AET/PET, the ratio of actual (AET) to potential (PET) evapotranspiration calculated from eddy-covariance measurements, as a proxy for soil water availability at monthly scale (Figure S2) (Chen et al., 2010; Gentine et al., 2007, 2011; Shinker and Bartlein, 2010) and vapour pressure deficit (VPD) as the atmospheric dryness proxy (Konings et al., 2017; Liu et al., 2020; Novick et al., 2016). We then calculated the correlation coefficient between monthly AET/PET and monthly VPD ($R_{constraints}$) (Fig. 1**B**). We used the ecosystem light-use efficiency (LUE_{EC}) as an indicator of forest photosynthesis capacity (Yuan et al., 2019) (Fig. 2, Supplementary Methods). For the pixel-based analysis at larger spatial scales, we calculated the canopy fluorescence yield (F_{qy}) of forest by dividing the satellite Solar Induced Fluorescence (SIF) by the absorbed photosynthetically active radiation (APAR), to examine the seasonal photosynthesis (Zeng et al., 2019) (Fig. 2, Supplementary Methods). We primarily focused on the warm season period from April to September and the data during the periods beyond these warm seasons were excluded from the data analysis (Supplementary Method).

2. Materials and Methods

Eddy-covariance and satellite-based data for plant photosynthesis. We mainly focused on forest ecosystems in the Northern Hemisphere with latitude > 15°N (Fig. 1**A**; Figure S1) and carried out the study by using monthly eddy-covariance observations from the FLUXNET 2015 openly available database (Tier 1) (Pastorello et al., 2020) and satellite-based GOME-2 (Global Ozone Monitoring Experiment-2) and TROPOMI (TROPOspheric Monitoring Instrument) SIF data. Additional satellite-based phenological data, e.g. NDVI (normalized difference vegetation index) (Wang et al., 2004), LAI (leaf area index) (Buermann et al., 2001), EVI (enhanced vegetation index, Didan, 2015), NIRv (near-infrared vegetation reflectance, Badgley et al., 2017) and Ku-VOD (Ku-band vegetation optical depth) (Fan et al. 2019), were also analyzed to examine the seasonal variations. Detailed methods for selecting eddy-covariance data and for calculating the ecosystem light use efficiency (LUE) were introduced in the Supplementary Methods.

Disentangling soil moisture deficits and atmospheric dryness effects on plant photosynthesis. Following Novick et al. (2016), if forest photosynthesis response to VPD varied significantly between different soil moisture bins, the site would be more soil-moisture limited; while if there were minimal changes in ecosystem conductance sensitivity to VPD across soil moisture bins, the site would be more VPD-limited. Here, we used monthly values of dryness index (AET/PET) as a proxy for seasonal soil water availability; and then investigated the relationship between LUE_{EC} and VPD increase for different AET/PET bins in negative and positive $R_{climate}$, respectively. Those with higher coefficients of variation (CV, Supplementary methods) of LUE_{EC} between different AET/PET bins under higher VPD were assumed to be less constrained by high atmospheric dryness, implying relatively more soil moisture limitations. On the contrary, those with lower CV of LUE_{EC} between different AET/PET bins under higher VPD were assumed to be more constrained by high atmospheric dryness, implying less soil moisture constraints.

We used Locally Weighted Regression Algorithm to fit the curves of LUE against VPD for each AET/PET bin (Fig. 3). Additionally, by comparing linear, log-linear, quadratic, and cubic spline functions, a cubic spline function with the lowest Akaike information criterion was selected to fit the curves. To test the significance of the relationship between soil water availability (or atmospheric dryness) and LUE_{EC}, the

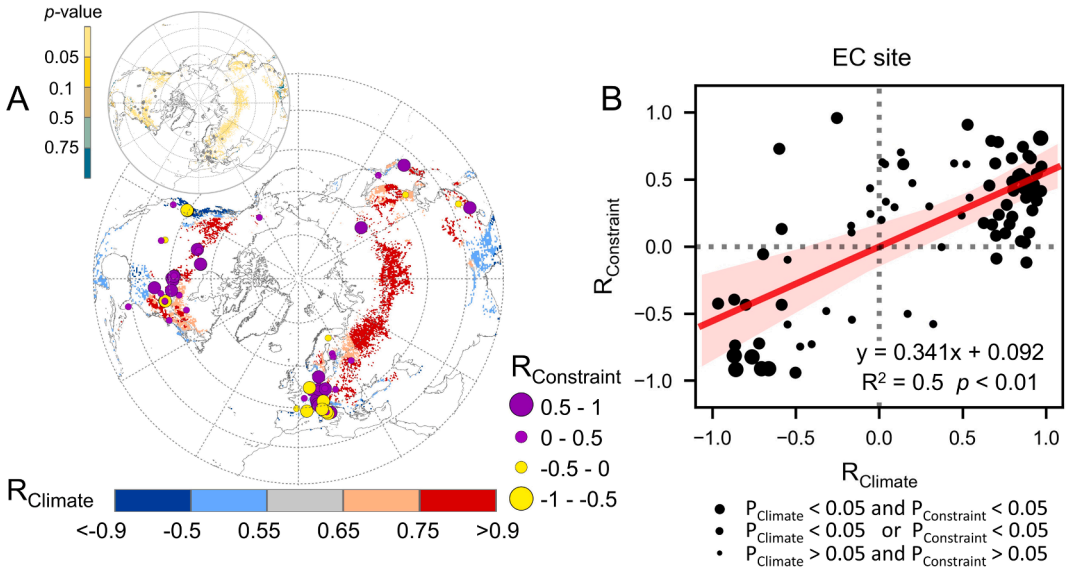

Fig. 1. Pearson coefficient between monthly mean precipitation (*Pre*) and monthly incoming shortwave radiation (*SW*) ($R_{climate}$) (background map in panel A) and Pearson coefficient between monthly vapor pressure deficit (VPD) and monthly ratio (AET/PET) of actual (ET) to potential evapotranspiration (PET) ($R_{constraint}$) (symbols in panel A) from April to September. Symbols represent the 83 eddy covariance forest sites in the Northern Hemisphere. Symbol size represents absolute R values and symbol color represents negative and positive values. Panel B represents the $R_{climate}$-$R_{constraint}$ scatterplot for the 83 sites.

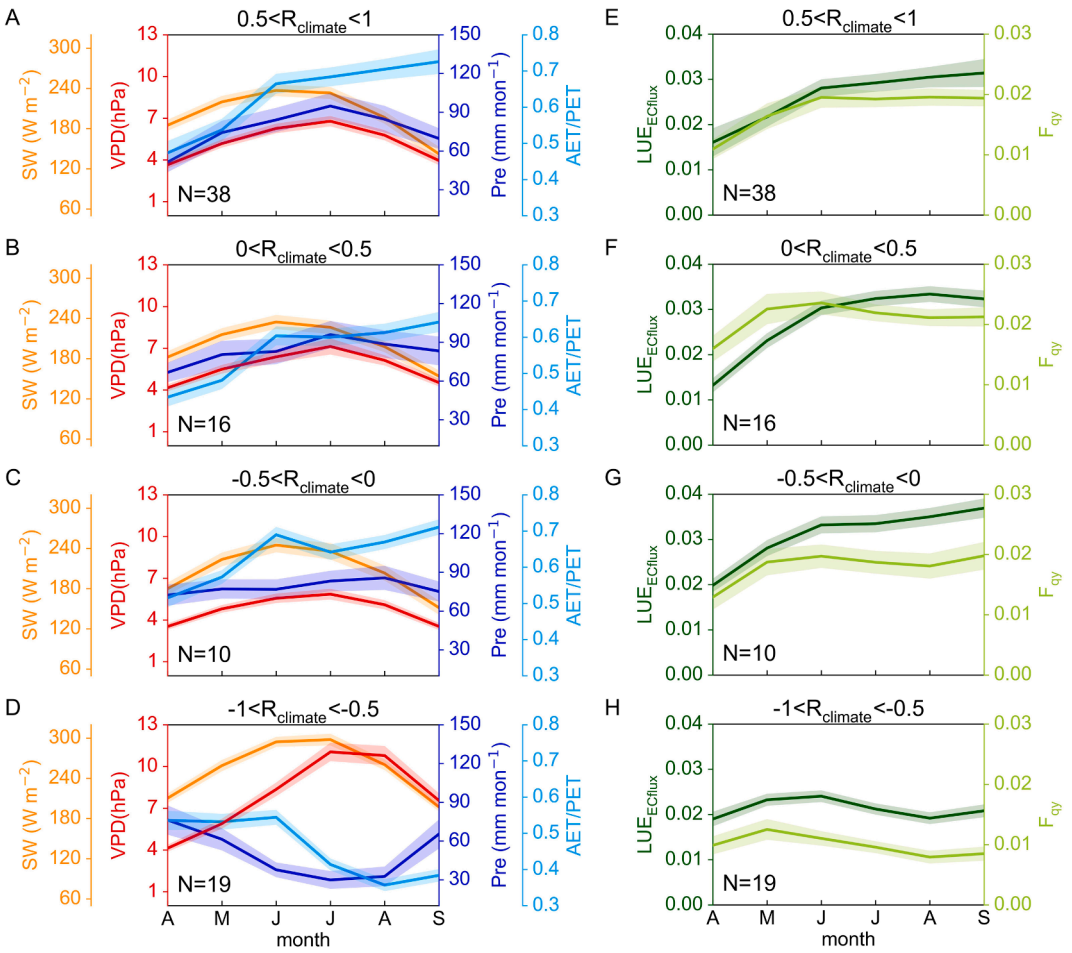

Fig. 2. Seasonal variability of climatic variables (panels A ~ D) and photosynthesis (E ~ H) for the Northern Hemisphere eddy covariance forest sites characterized by $R_{climate} > 0.5$ (A, E), $0 < R_{climate} < 0.5$ (B, F), $-0.5 < R_{climate} < 0$ (C, G), and $R_{climate} < -0.5$ (D, H). $R_{climate}$ is the correlation between monthly mean precipitation (*Pre*) and monthly incoming shortwave radiation (*SW*) during the growing season (April-September). Climate variables include SW, Pre, vapor pressure deficit (VPD), and ratio (AET/PET) of actual (AET) to potential evapotranspiration (PET). Photosynthetic variables include light use efficiency calculated using eddy covariance data (LUE_{EC}) and remotely sensed quantum yield of fluorescence (F_{qy}) (see **Supplementary Methods**). Non-growing season months are excluded.

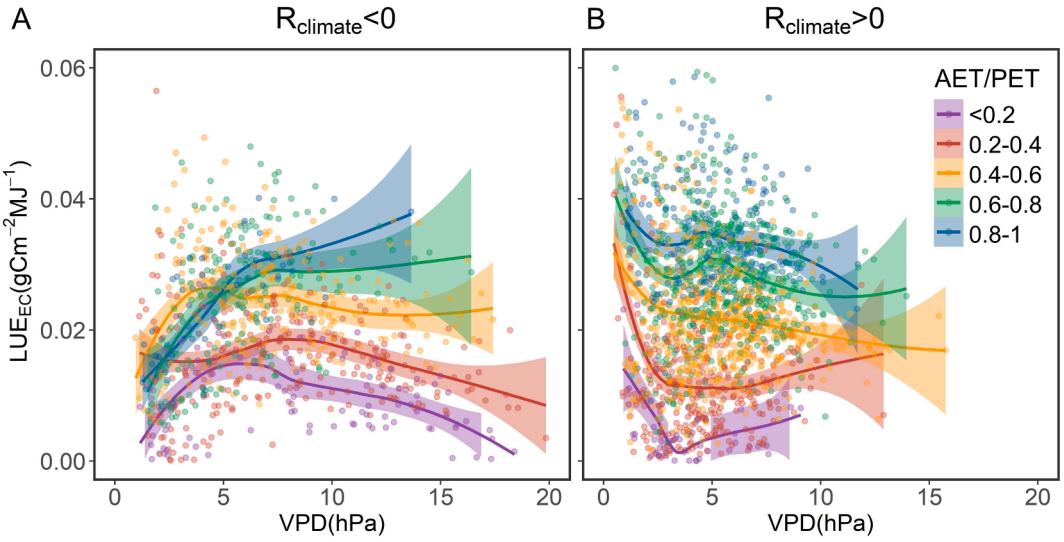

Fig. 3. Scatter diagrams between monthly ecosystem light-use efficiency (LUE_{EC}) and vapour pressure deficit (VPD) of 83 eddy-covariance sites with different AET/PET bins. The LUE_{EC} is calculated from gross primary production, divided by the absorbed photosynthetically active radiation. Panels A and B are LUE_{EC} against VPD for $R_{climate} < 0$ and $R_{climate} > 0$ for eddy-covariance sites. The curves were fitted by using the locally weighted regression. The shaded area represents the 95% confidence interval.

p values of the correlation between soil moisture (or VPD) and LUE_{EC} seasonality were calculated for each VPD bin using a mixed-effect linear model, in the R package lme4 (Bates et al., 2015). A smaller *p* value implied a more significant relationship; while a bigger *p* value implied a weaker relationship. We used $p = 0.05$ as the criteria for detecting the significance level of the correlations in this study. A piecewise linear model was performed to objectively identify the inflection point of the relationship between VPD and LUE using the bootstrap restarting algorithm implemented in the R package SiZer (Sonderegger et al., 2009). This inflection point reflects the position in the curve where the correlations between VPD and LUE shifted to another slope. All statistical analyses were performed in R v.4.0.2.

3. Results

3.1. Strong atmospheric water constraints on forest photosynthesis under synchronous climate

Among the 83 eddy-covariance forest sites (Fig. 1**A**), $R_{climate}$ values are positively correlated with $R_{constraint}$ (correlation between VPD and AET/PET) values (Fig. 1**B**). The multi-year mean seasonality (12 months) of *Pre* shows a downward parabolic curve in most sites (32 out of 44) with $0.0 < R_{climate} < 1.0$ (Fig. 2 A and B), and gradually changes to an upward parabolic curve (12 out of 19) with most sites where $-1.0 < R_{climate} < -0.5$ (Fig. 2 D) (Figure S1). The forests with stronger positive values of $R_{climate}$ between monthly *Pre* and *SW* (red color, Fig. 1**A**), i.e. with strong in phase seasonality (Fig. 2), also have larger positive values of $R_{constraint}$ (purple circles, Fig. 1**A**) between monthly AET/PET and VPD (Fig. 1**B**). In drier seasons, the AET/PET, a proxy for soil water content (Figure S2), is lower when atmospheric demand for water (i.e. VPD) is also smaller (Fig. 2**A** and **B**). In wetter seasons, VPD is higher when soil water is sufficient for this stronger atmospheric demand for water. This implies that those sites likely exhibit very mild seasonal water stress; and the low soil moisture and high atmospheric dryness potentially limit forest photosynthesis in different seasons. On the contrary, forests with stronger negative values of $R_{climate}$ between monthly *Pre* and *SW* (blue color, Fig. 1**A**), i.e. with strong anti-phase seasonality (Fig. 2), usually have negative values of $R_{constraint}$ (yellow circles, Fig. 1**A**) i.e. anti-correlation between AET/PET and VPD (Fig. 1**B**). This implies that low soil moisture and high atmospheric dryness limit forest photosynthesis during the same season. In drier seasons, the AET/PET is usually lower when it is companied by higher VPD (Fig. 2**D**). In that case, those sites with strong negative $R_{climate}$ also exhibit strong seasonal water stress from both soil water deficits and atmospheric water deficits.

Our analyses of seasonal LUE_{EC} for different $R_{climate}$ support above inferences. Forests exhibit higher LUE_{EC} (Fig. 2**E, F and G, see** Supplementary Methods) under $R_{climate} > -0.5$ in July and August, with higher monthly *Pre*, AET/PET and VPD (Fig. 2**A, B and C)**; but forests show lower LUE_{EC} under $R_{climate} < -0.5$ in July and August (Fig. 2 **H)**, with lower monthly *Pre*, AET/PET and higher monthly VPD (Fig. 2 **D)**. In July and August, the F_{qy} (light green curves in Fig. 2) and most satellite-based photosynthetic proxies (**Figure S3**) also have higher values under $R_{climate} > -0.5$ than under $R_{climate} < -0.5$. This can be quantitatively reflected by the regression slopes of relationships between monthly LUE_{EC} (or F_{qy}) and months. Result shows more positive values for sites with larger $R_{climate}$ from April to September and more negative values for sites with smaller $R_{climate}$ (**Figure S4**).

We calculated the CV of LUE_{EC} for different bins of VPD (**Supplementary Methods**). For sites where $R_{climate} < 0$, results show that the CV values firstly drop as VPD increases but then increase after VPD is>10 hPa (**Figure S5A**). While, for sites where $R_{climate} > 0$, the CV values always decrease as VPD increases (**Figure S5B**). Fig. 3 presents the relationship between LUE_{EC} and VPD in different AET/PET bins fitted by both the locally weighted regression and cubic spline function (see **Supplementary Methods**). For sites with $R_{climate} < 0$, the LUE_{EC} firstly increases as VPD increases under low VPD conditions (VPD < ~5.0 hPa) and then decreases (for low soil water contents) or stays stable (for higher soil water contents) when VPD becomes higher (Fig. 3**A**). For sites with $R_{climate} > 0$, the LUE_{EC} firstly decreases continuously as VPD increases (Fig. 3**B**). It is interesting to see that our finding from sites with $R_{climate} < 0$ is consistent with the results of Zhou et al. (2015), which showed that increases in VPD significantly promoted photosynthesis when VPD was at a low value and inhibited photosynthesis when VPD was high. This is probably because the VPD rising is due to temperature warming and increased temperature promotes photochemistry (Drake et al., 2017) and may also trigger new leaf flush to increase photosynthesis capacity when there is rare soil water stress. Notably, the LUE_{EC} diverges with higher CV across different AET/PET bins when VPD becomes higher for sites with $R_{climate} < 0$, while LUE_{EC} converges with lower CV between different AET/PET bins when VPD becomes higher for sites with $R_{climate} > 0$. Similar results are found when using the locally weighted regression (**Figure S6**). These results indicate a weaker atmospheric water constraint on LUE_{EC} where $R_{climate} < 0$ but a stronger atmospheric water constraint on LUE_{EC} where $R_{climate} > 0$ (**see Supplementary Methods**). We further calculated the *p* values of the dependence of LUE_{EC} on soil moisture and VPD for each VPD segments using a mixed-effect linear model (**Figure S7**). For sites with $R_{climate} < 0$, LUE_{EC} is significantly influenced by AET/PET (*p* value < 0.01), but it is less correlated to VPD (*p* value > 0.01). There is a similar pattern for sites with $R_{climate} > 0$, but under higher VPD conditions LUE_{EC} is significantly influenced by VPD (*p* value < 0.01). These analyses support the idea that sites where $R_{climate} > 0$ exhibit stronger atmospheric dryness constraints on forest ecosystem under higher VPD conditions.

3.2. Spatial patterns across the Northern Hemisphere

At the continental scale, we analyzed the forest areas using the MODIS land cover products (MCD12C1) (Sulla-Menashe & Friedl, 2018). We calculated pixel-based $R_{climate}$ of forestlands (**map,** Fig. 1**A**) to further test our hypothesis that strong positive $R_{climate}$ also exhibits strong positive $R_{constraint}$ values and show strong seasonal atmospheric water constraints on forest ecosystem. Results reveal that higher latitudes show larger positive values of $R_{climate}$ between monthly *Pre* and *SW* (**Figure S8**). The monthly differences in F_{qy} (ΔF_{qy}) during warm seasons are shown in Fig. 4. The ΔF_{qy} are strongly related to $R_{climate}$. Larger $R_{climate}$ show larger positive values of ΔF_{qy} from April to June, while larger $R_{climate}$ show more negative values of ΔF_{qy} from July to September. Our pixel-based analyses suggest no water constraint or slight water constraints on F_{qy} under positive $R_{climate}$ during the early-to-mid stage of the growing seasons (April to July). The Fqy then peaks in July and temperature increases to the optimal values for plant photosynthesis, when there is still rare water constraint from atmospheric dryness. But results show stronger water constraints on F_{qy} during the end of growing season (around July to September).

4. Discussion

Although soil water availability and atmospheric dryness both govern stomatal closure to regulate plant photosynthesis (Konings and Gentine, 2016; Konings et al., 2017), understanding in which kind of climates forests are more sensitive to either soil water availability or atmospheric dryness or both is widely debated (Lobell et al., 2014; Zhou et al., 2019b). A recent study based on SIF data showed that soil water availability controlled global vegetation photosynthesis over larger areas than atmospheric dryness (Liu et al., 2020). However, these results were derived without removing the coincident impacts of photosynthetically active radiation and absorbed fraction of photosynthetically active radiation (Lu et al., 2022). By eliminating those parts of effects, Lu et al. (2022) found that atmospheric dryness rather than soil water availability dominated plant photosynthesis over more flux sites and larger areas globally. Here, our findings showed clearly the spatial

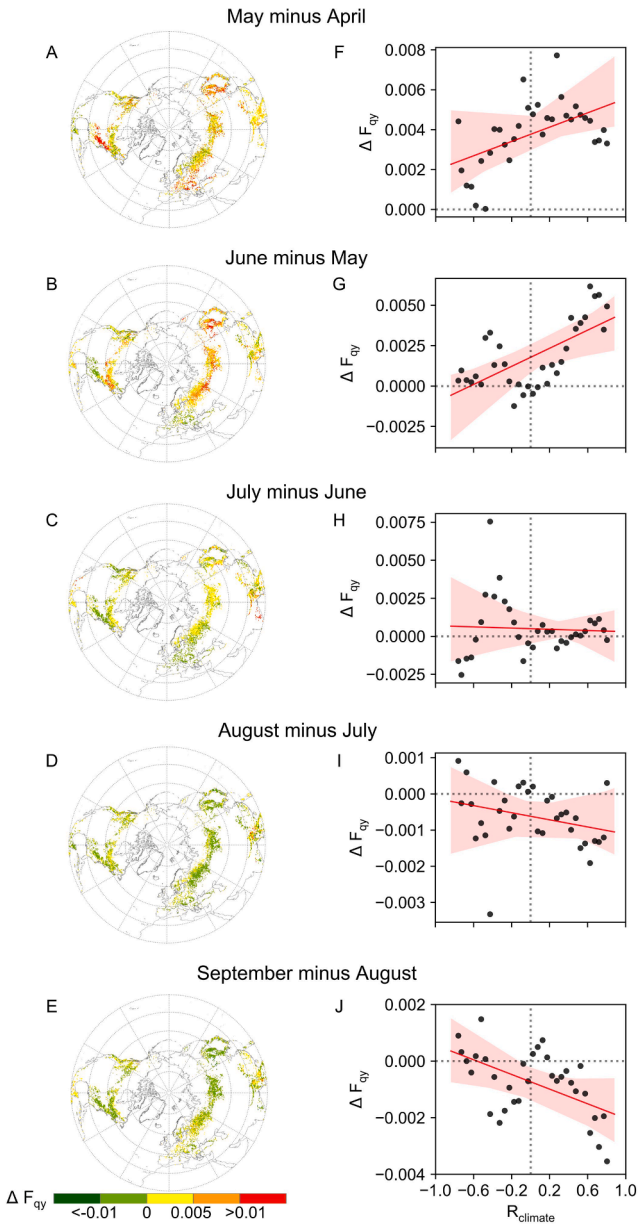

Fig. 4. Monthly variations in remotely sensed quantum yield of fluorescence (F_{qy}) (see **Supplementary Methods**) during warm seasons (April-September). The F_{qy} is calculated by dividing the satellite-based solar induced fluorescence by the absorbed photosynthetically active radiation. ΔF_{qy} is calculated by using the F_{qy} of a later month minus F_{qy} of a former month, which are labeled as names of the later month minus that of the former month in the plots. The non-growing seasons are exclude.

patterns of soil water availability and atmospheric dryness -dominated ecoregions. The mid-to-high latitude forests with negative $R_{climate}$ usually encountered co-occurring high VPD and low AET/PET stresses. The inflection point analysis of VPD against LUE (**Methods**) shows that the thresholds (V_t) of VPD for partitioning the sites under water stress increases as AET/PET increases (**Figure S9A**). The sensitivity of LUE_{EC} to VPD is small for all AET/PET levels (**Figure S9C**). These analyses support that ecosystems with negative $R_{climate}$ usually display weaker atmospheric dryness stress and stronger soil moisture constraint on forest photosynthesis. However, for forests with positive $R_{climate}$, the V_t values vary slightly around 7.0 for various AET/PET levels (**Figure S9B**). But the sensitivity of LUE_{EC} to VPD decreases from positive values to negative values as AET/PET increases (**Figure S9D**). These results imply that forests with $R_{climate} > 0$ show strong atmospheric dryness dependence of photosynthesis. These forests exhibit higher seasonal photosynthesis throughout the whole growing season than other forest types. Over the globe, terrestrial pixels with $R_{climate} > 0$ showed larger coverage (68%) than those with $R_{climate} < 0$ (32%) (**Figure S10**). This implied strong atmospheric water constraints on terrestrial forest photosynthesis, similar with the conclusion of Lu et al. (2022). With increased global VPD (Yuan et al., 2019), the ecoregions controlled by high atmospheric dryness might be expanded in the future.

We also note that the influences of atmospheric dryness on plant photosynthesis capacity is strongly related to the level of AET/PET (Fig. 3). It is interesting that, only for $R_{climate} < 0$ where precipitation and radiation availability happens in different seasons, there is positive increase of LUE_{EC} with VPD when VPD < 5.0 hPa or at wetter conditions AET/PET > 0.4, and a parabolic response of LUE_{EC} to VPD at drier conditions, with a decrease at high VPD when VPD > 5.0 hPa (Fig. 3**A**). This implies that under wet conditions, there is sufficient soil water supply for atmospheric water demands where energy is limited. Plant photosynthesis is rarely limited with VPD increases; on the contrary, plant photosynthesis increases as climate becomes warmer in the growing seasons. Under drier conditions, high VPD will force plants to prevent excessive water loss, which in turn inhibits leaf photosynthesis (Cowan and Farquhar, 1977; Oren et al., 1999; McAdam and Brodribb, 2015). This can also be reflected by the negative correlation between AET/PET and the Bowen ratio (**Figure S11A**). When the Bowen ratio becomes very large, the surface has very little water to be transpired into atmosphere and evaporation is mostly dependent on available energy (i.e., atmospheric demands for water). Conversely, when the Bowen ratio becomes very small, it is in wet areas and there are rare limitations on the removal of surface water into atmosphere. The evapotranspiration is more dependent on the supply of unsaturated atmospheric air (i.e., soil water supply) (Dickinson, 1995; Hartmann, 2009). So, forests with a smaller Bowen ratio, usually with higher AET/PET ratio, show larger average photosynthesis capacities than those with a higher Bowen ratio (i.e. lower AET/PET) (**Figure S11B**).

Our analyses point to the importance of the coupling of rainfall and radiation in influencing the responses of forest photosynthesis to variability of soil water and atmospheric dryness. It provides a better understanding of the coupled terrestrial carbon uptakes, energy exchanges, and water transfers. Ignoring these differences in low soil moisture and high atmospheric dryness constraints on forest photosynthesis in different radiation-rainfall coupling climates will lead to incorrect projections of plant phenological and physiological responses to ongoing climate change. However, the effects of seasonal temperature disturbances on forest photosynthesis are not excluded when exploring the soil and atmospheric water constraints. This might bring uncertainty and needs further in-depth studies.

Declaration of Competing Interest

The authors declare that they have no known competing financial interests or personal relationships that could have appeared to influence the work reported in this paper.

Acknowledgement

This study was supported by the National Natural Science Foundation of China [grant numbers 31971458, 41971275, 41907289], Special high-level plan project of Guangdong Province [grant number 2016TQ03Z354], the Natural Science Foundation of Guangdong [grant number 2020A1515010910], and the 'GDAS' project of Science and Technology Development [grant number 2020GDASYL-20200102002]. This work used eddy covariance data acquired and shared by the FLUXNET community, including the following networks: AmeriFlux, AfriFlux, AsiaFlux, CarboAfrica, CarboEuropeIP, CarboItaly, CarboMont, ChinaFlux, Fluxnet-Canada, GreenGrass, ICOS, KoFlux, LBA,

NECC, OzFlux-TERN, TCOS-Siberia, and USCCC. The FLUXNET eddy covariance data processing and harmonization was carried out by the ICOS Ecosystem Thematic Center, AmeriFlux Management Project, and Fluxdata project of FLUXNET, with the support of CDIAC, and the OzFlux, ChinaFlux, and AsiaFlux offices.

Data availability

Data archiving is underway. We plan to use ZENODO repository to upload a copy of our data. We are now providing the supporting Information for review purposes. Once accepted, the data will be availability in ZENODO repository.

Contributions

Y.S. and P.C. designed the study. Y.S. and X.Q. collected and analyzed the data and elaborated the figures. All authors contributed to writing and editing the text and discussing the scientific questions.

Appendix A. Supplementary material

Supplementary data to this article can be found online at https://doi.org/10.1016/j.jag.2022.102808.

References

Badgley, G., Field, C.B., Berry, J.A., 2017. Canopy near-infrared reflectance and terrestrial photosynthesis. Sci. Adv. 3 (3), e1602244. https://doi.org/10.1126/sciadv.1602244.

Bates, D., Mächler, M., Bolker, B., Walker, S., 2015. Fitting linear mixed-effects models using lme4. J. Stat. Softw. 67 (1), 1–48. https://doi.org/10.18637/jss.v067.i01.

Buermann, W., Dong, J., Zeng, X., Myneni, R.B., Dickinson, R.E., 2001. Evaluation of the utility of satellite-based leaf area index data for climate simulation. J. Clim. 14, 3536–3550.

Chen, L., Wang, J., Wei, W., Fu, B., Wu, D., 2010. Effects of landscape restoration on soil water storage and water use in the Loess Plateau Region, China. For. Ecolo. Manage. 259 (7), 1291–1298.

Cheng, L., Zhang, L., Wang, Y., Canadell, J.G., Chiew, F.H.S., Beringer, J., Li, L., Miralles, D.G., Piao, S., Zhang, Y., 2017. Recent increases in terrestrial carbon uptake at little cost to the water cycle. Nat. Commun. 8, 110. https://doi.org/10.1038/s41467-017-00114-5.

Cowan, I.R., Farquhar, G.D., 1977. Stomatal function in relation to leaf metabolism and environment. Symp. Soc. Exp. Biol. 31, 471–505.

Didan, K. (2015). MOD13C2 MODIS/Terra vegetation indices monthly L3 global 0.05deg CMG V006 [Data Set] (NASA EOSDIS LP DAAC). 10.5067/MODIS/MOD13C2.006.

Ding, J., Yang, T., Zhao, Y., Liu, D., Wang, X., Yao, Y., Peng, S., Wang, T., Piao, S., 2018. Increasingly important role of atmospheric aridity on Tibetan alpine grasslands. Geophys. Res. Lett. 45 (6), 2852–2859. https://doi.org/10.1002/2017GL076803.

Dickinson, R.E., 1995. Land-atmosphere interaction. Rev. Geophys. 33 (S2), 917–922. https://doi.org/10.1029/95RG00284.

Drake, J.E., Vårhammar, A., Kumarathunge, D., Medlyn, B.E., Pfautsch, S., Reich, P.B., Tissue, D.T., Ghannoum, O., Tjoelker, M.G., 2017. A common thermal niche among geographically diverse populations of the widely distributed tree species Eucalyptus tereticornis: No evidence for adaptation to climate-of-origin. Glob. Change Biol. 23 (12), 5069–5082.

Fan, L., Wigneron, J.-P., Ciais, P., Chave, J., Brandt, M., Fensholt, R., Saatchi, S.S., Bastos, A., Al-Yaari, A., Hufkens, K., Qin, Y., Xiao, X., Chen, C., Myneni, R.B., Fernandez-Moran, R., Mialon, A., Rodriguez-Fernandez, N.J., Kerr, Y., Tian, F., Peñuelas, J., 2019. Satellite-observed pantropical carbon dynamics. Satellite-observed pantropical carbon dynamics. Nat. Plants 5 (9), 944–951. https://doi.org/10.1038/s41477-019-0478-9.

Gentine, P., Entekhabi, D., Polcher, J., 2011. The diurnal behavior of evaporative fraction in the soil–vegetation–atmospheric boundary layer continuum. J. Hydrometeorol. 12 (6), 1530–1546.

Gentine, P., Entekhabi, D., Chehbouni, A., Boulet, G., Duchemin, B., 2007. Analysis of evaporative fraction diurnal behaviour. Agric. For. Meteorol. 143 (1-2), 13–29.

Hartmann, D.L., 2009. Global Physical Climatology. Chapter: The Hydrological Cycle. http://doi.org/10.1016/B978-0-12-328531-7.00005-0.

Katul, G.G., Palmroth, S., Oren, R., 2009. Leaf stomatal responses to vapour pressure deficit under current and CO2-enriched atmosphere explained by the economics of gas exchange. Plant, Cell Environ. 32, 968–979. https://doi.org/10.1111/j.1365-3040.2009.01977.x.

Konings, A.G., Williams, A.P., Gentine, P., 2017. Sensitivity of grassland productivity to aridity controlled by stomatal and xylem regulation. Nat. Geosci. 10 (4), 284–288. https://doi.org/10.1038/ngeo2903.

Konings, A.G., Gentine, P., 2017. Global variations in ecosystem-scale isohydricity. Glob. Change Biol. 23 (2), 891–905. https://doi.org/10.1111/gcb.13389.

Liu, L., Gudmundsson, L., Hauser, M., Qin, D., Li, S., Seneviratne, S.I., 2020. Soil moisture dominates dryness stress on ecosystem production globally. Nat. Commun. 11 (1), 1–9.

Lobell, D.B., Roberts, M.J., Schlenker, W., Braun, N., Little, B.B., Rejesus, R.M., Hammer, G.L., 2014. Greater sensitivity to drought accompanies maize yield increase in the U.S. Midwest. Science 344 (6183), 516–519.

Lu, H., Qin, Z., Lin, S., Chen, X., Chen, B., He, B., Wei, J., Yuan, W., 2022. Large influence of atmospheric vapor pressure deficit on ecosystem production efficiency. Nat. Commun. 13 (1) https://doi.org/10.1038/s41467-022-29009-w.

Martínez-Vilalta, J., Garcia-Forner, N., 2017. Water potential regulation, stomatal behaviour and hydraulic transport under drought: Deconstructing the iso/anisohydric concept. Plant, Cell Environ. 40 (6), 962–976.

Martínez-Vilalta, J., Poyatos, R., Aguadé, D., Retana, J., Mencuccini, M., 2014. A new look at water transport regulation in plants. New Phytol. 204 (1), 105–115. https://doi.org/10.1111/nph.12912.

McAdam, S.A.M., Brodribb, T.J., 2015. The evolution of mechanisms driving the stomatal response to vapor pressure deficit. Plant Physiol. 167 (3), 833–843.

Messori, G., Ruiz-Pérez, G., Manzoni, S., Vico, G., 2019. Climate drivers of the terrestrial carbon cycle variability in Europe. Environ. Res. Lett. 14 (6), 063001. https://doi.org/10.1088/1748-9326/ab1ac0.

Novick, K.A., Ficklin, D.L., Stoy, P.C., Williams, C.A., Bohrer, G., Oishi, A.C., Papuga, S.A., Blanken, P.D., Noormets, A., Sulman, B.N., Scott, R.L., Wang, L., Phillips, R.P., 2016. The increasing importance of atmospheric demand for ecosystem water and carbon fluxes. Nat. Clim. Change 6 (11), 1023–1027. https://doi.org/10.1038/nclimate3114.

Oren, R., Sperry, J.S., Katul, G.G., Pataki, D.E., Ewers, B.E., Phillips, N., Schäfer, K.V.R., 1999. Survey and synthesis of intra- and interspecific variation in stomatal sensitivity to vapour pressure deficit. Plant, Cell Environ. 22, 1515–1526.

Pastorello, G., Trotta, C., Canfora, E., Chu, H., Christianson, D., Cheah, Y., Poindexter, C., Chen, J., Elbashandy, A., Humphrey, M., Isaac, P., Polidori, D., Reichstein, M., Ribeca, A., van Ingen, C., Vuichard, N., Zhang, L., Amiro, B., Ammann, C., Arain, M. A., Ardö, J., Arkebauer, T., Arndt, S. K., Arriga, N., Aubinet, M., Aurela, M., Baldocchi, D., Barr, A., Beamesderfer, E., Marchesini, L. B., Bergeron, O., Beringer, J., Bernhofer, C., Berveiller, D., Billesbach, D., Black, T. A., Blanken, P. D., Bohrer, G., Boike, J., Bolstad, P. V., Bonal, D., Bonnefond, Jean-M., Bowling, D. R., Bracho, R., Brodeur, J., Brümmer, C., Buchmann, N., Burban, B., Burns, S. P., Buysse, P., Cale, P., Cavagna, M., Cellier, P., Chen, S., Chini, I., Christensen, T. R., Cleverly, J., Collalti, A., Consalvo, C., Cook, B. D., Cook, D., Coursolle, C., Cremonese, E., Curtis, P. S., D'Andrea, E., da Rocha, H., Dai, X., Davis, K. J., Cinti, B. D., Grandcourt, A. D., Ligne, A. D., De Oliveira, R. C., Delpierre, N., Desai, A. R., Di Bella, C. M., Tommasi, P. D., Dolman, H., Domingo, F., Dong, G., Dore, S., Duce, P., Dufrêne, E., Dunn, A., Dušek, J., Eamus, D., Eichelmann, U., ElKhidir, H. A. M., Eugster, W., Ewenz, C. M., Ewers, B., Famulari, D., Fares, S., Feigenwinter, I., Feitz, A., Fensholt, R., Filippa, G., Fischer, M., Frank, J., Galvagno, M., Gharun, M., Gianelle, D., Gielen, B., Gioli, B., Gitelson, A., Goded, I., Goeckede, M., Goldstein, A. H., Gough, C. M., Goulden, M. L., Graf, A., Griebel, A., Gruening, C., Grünwald, T., Hammerle, A., Han, S., Han, X., Hansen, B. U., Hanson, C., Hatakka, J., He, Y., Hehn, M., Heinesch, B., Hinko-Najera, N., Hörtnagl, L., Hutley, L., Ibrom, A., Ikawa, H., Jackowicz-Korczynski, M., Janouš, D., Jans, W., Jassal, R., Jiang, S., Kato, T., Khomik, M., Klatt, J., Knohl, A., Knox, S., Kobayashi, H., Koerber, G., Kolle, O., Kosugi, Y., Kotani, A., Kowalski, A., Kruijt, B., Kurbatova, J., Kutsch, W. L., Kwon, H., Launiainen, S., Laurila, T., Law, B., Leuning, R., Li, Y., Liddell, M., Limousin, J. M., Lion, M., Liska, A. J., Lohila, A., López-Ballesteros, A., López-Blanco, E., Loubet, B., Loustau, D., Lucas-Moffat, A., Lüers, J., Ma, S., Macfarlane, C., Magliulo, V., Maier, R., Mammarella, I., Manca, G., Marcolla, B., Margolis, H. A., Marras, S., Massman, W., Mastepanov, M., Matamala, R., Matthes, J. H., Mazzenga, F., McCaughey, H., McHugh, I., McMillan, A. M. S., Merbold, L., Meyer, W., Meyers, T., Miller, S. D., Minerbi, S., Moderow, U., Monson, R. K., Montagnani, L., Moore, C. E., Moors, E., Moreaux, V., Moureaux, C., Munger, J. W., Nakai, T., Neirynck, J., Nesic, Z., Nicolini, G., Noormets, A., Northwood, M., Nosetto, M., Nouvellon, Y., Novick, K., Oechel, W., Olesen, J. E., Ourcival, J. M., Papuga, S. A., Parmentier, F. J., Paul-Limoges, E., Pavelka, M., Peichl, M., Pendall, E., Phillips, R. P., Pilegaard, K., Pirk, N., Posse, G., Powell, T., Prasse, H., Prober, S. M., Rambal, S., Rannik, Ü., Raz-Yaseef, N., Rebmann, C., Reed, D., Dios, V. R., Restrepo-Coupe, N., Reverter, B. R., Roland, M., Sabbatini, S., Sachs, T., Saleska, S. R., Sánchez-Cañete, E. P., Sanchez-Mejia, Z. M., Schmid, H. P., Schmidt, M., Schneider, K., Schrader, F., Schroder, I., Scott, R. L., Sedlák, P., Serrano-Ortíz, P., Shao, C., Shi, P., Shironya, I., Siebicke, L., Šigut, L., Silberstein, R., Sirca, C., Spano, D., Steinbrecher, R., Stevens, R. M., Sturtevant, C., Suyker, A., Tagesson, T., Takanashi, S., Tang, Y., Tapper, N., Thom, J., Tomassucci, M., Tuovinen, J. P., Urbanski, S., Valentini, R., van der Molen, M., van Gorsel, E., van Huissteden, K., Varlagin, A., Verfaillie, J., Vesala, T., Vincke, C., Vitale, D., Vygodskaya, N., Walker, J. P., Walter-Shea, E., Wang, H., Weber, R., Westermann, S., Wille, C., Wofsy, S., Wohlfahrt, G., Wolf, S., Woodgate, W., Li, Y., Zampedri, R., Zhang, J., Zhou, G., Zona, D., Agarwal, D., Biraud, S., Torn, M., Papale, D., 2020. The FLUXNET2015 dataset and the ONEFlux processing pipeline for eddy covariance data. Scientific Data, 7(225), doi: org/10.1038/s41597-020-0534-3.

Shinker, J.J., Bartlein, P.J., 2010. Spatial variations of effective moisture in the western United States. Geophys. Res. Lett. 37 (2), n/a–n/a.

Sonderegger, D.L., Wang, H., Clements, W.H., Noon, B.R., 2009. Using SiZer to detect thresholds in ecological data. Front. Ecol. Environ. 7 (4), 190–195.

Sperry, J.S., Venturas, M.D., Anderegg, W.R.L., Mencuccini, M., Mackay, D.S., Wang, Y., Love, D.M., 2017. Predicting stomatal responses to the environment from the optimization of photosynthetic gain and hydraulic cost. Plant, Cell Environ. 40 (6), 816–830.

Sulla-Menashe, D., Friedl, M. A., 2018. User Guide to Collection 6 MODIS Land Cover (MCD12Q1 and MCD12C1) Product. USGS: Reston, VA, USA.

Tyree, M.T., Sperry, J.S., 1989. Vulnerability of xylem to cavitation and embolism. Annu. Rev. Plant Biol. 40 (1), 19–36.

Wang, C.-C., Chen, G.-J., Carbone, R.E., 2004. A Climatology of Warm-Season Cloud Patterns over East Asia Based on GMS Infrared Brightness Temperature Observations. Mon. Weather Rev. 132 (7), 1606–1629.

Yang, X., Wu, J., Chen, X., Ciais, P., Maignan, F., Yuan, W., Piao, S., Yang, S., Gong, F., Su, Y., Dai, Y., Liu, L., Zhang, H., Bonal, D., Liu, H., Chen, G., Lu, H., Wu, S., Fan, L., Gentine, P., Wright, S.J., 2021. A comprehensive framework for seasonal controls of leaf abscission and productivity in evergreen broadleaved tropical and subtropical forests. The Innovation 2 (4), 100154. https://doi.org/10.1016/j.xinn.2021.100154.

Yuan, W., Zheng, Y.i., Piao, S., Ciais, P., Lombardozzi, D., Wang, Y., Ryu, Y., Chen, G., Dong, W., Hu, Z., Jain, A.K., Jiang, C., Kato, E., Li, S., Lienert, S., Liu, S., Nabel, J.E. M.S., Qin, Z., Quine, T., Sitch, S., Smith, W.K., Wang, F., Wu, C., Xiao, Z., Yang, S., 2019. Increased atmospheric vapor pressure deficit reduces global vegetation growth. Science. Advances 5 (8). https://doi.org/10.1126/sciadv.aax1396.

Zeng, Y., Badgley, G., Dechant, B., Ryu, Y., Chen, M., Berry, J.A., 2019. A practical approach for estimating the escape ratio of near-infrared solar-induced chlorophyll fluorescence. Remote Sens. Environ. 232, 111209. https://doi.org/10.1016/j.rse.2019.05.028.

Zhou, G., Wei, X., Chen, X., Zhou, P., Liu, X., Xiao, Y., Sun, G., Scott, D.F., Zhou, S., Han, L., Su, Y., 2015. Global pattern for the effect of climate and land cover on water yield. Nat. Commun. 6 (1) https://doi.org/10.1038/ncomms6918.

Zhou, S., Williams, A.P., Berg, A., Cook, B.I., Zhang, Y., Hagemann, S., Lorenz, R., Seneviratne, S.I., Gentine, P., 2019a. Land-atmosphere feedbacks exacerbate concurrent soil drought and atmospheric aridity. PNAS 116 (38), 18848–18853. https://doi.org/10.1073/pnas.1904955116.

Zhou, S., Zhang, Y., Williams, A.P., Gentine, P., 2019b. Projected increases in intensity, frequency, and terrestrial carbon costs of compound drought and aridity events. Sci. Adv. 5 (1) https://doi.org/10.1126/sciadv.aau5740.